



issn: 1600-5767 journals.iucr.org/j

# **RamPlot**: a webserver to draw 2D, 3D and assorted Ramachandran ( $\varphi$ , ψ) maps

Mayank Kumar and R. S. Rathore

J. Appl. Cryst. (2025). 58, 630–636



Author(s) of this article may load this reprint on their own web site or institutional repository and on not-for-profit repositories in their subject area provided that this cover page is retained and a permanent link is given from your posting to the final article on the IUCr website.

For further information see https://journals.iucr.org/services/authorrights.html



ISSN 1600-5767

Received 7 October 2024 Accepted 22 February 2025

Edited by J. Hajdu, Uppsala University, Sweden and The European Extreme Light Infrastucture, Czechia

**Keywords:** torsion-angle  $(\varphi, \psi)$  maps; protein conformations; main chain conformations; Ramachandran maps.

**Supporting information:** this article has supporting information at journals.iucr.org/j

## *RamPlot*: a webserver to draw 2D, 3D and assorted Ramachandran ( $\varphi$ , $\psi$ ) maps

Mayank Kumar and R. S. Rathore\*

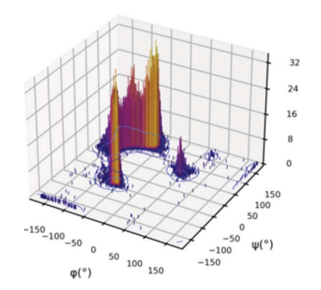
Department of Bioinformatics, School of Earth Biological and Environmental Sciences, Central University of South Bihar, Gaya, 824236, India. \*Correspondence e-mail: rsrathore@cusb.ac.in

The Ramachandran steric map of torsion angles  $(\varphi, \psi)$  introduced in 1963 has been widely used for protein structure validation and model building. Many developments in the field have made it essential to develop a utility to plot assorted types of maps for the following specific reasons: (i) to investigate different types (Gly, Val/Ile, pre/trans/cis-Pro and general) of 2D and 3D maps, addressing the diverse steric environments and frequency distribution of conformations, (ii) to examine polypeptides containing non-standard residues, (iii) for better visualization and analysis of conformational excursions and transitions in simulation, and (iv) to analyse torsion angles across three rotatable bonds such as preferred backbone-dependent rotamers. The utility RamPlot is accessible online (https://www.ramplot.in) and offline (via GitHub, https://github.com/mayank2801/ramplot and PyPI repository). It serves as a unique tool to draw and interpret a great variety of Ramachandran maps for natural and non-standard residues, which is otherwise unfeasible using existing tools and servers.

#### 1. Introduction

The Ramachandran  $(\varphi, \psi)$  steric map, introduced in 1963 by G. N. Ramachandran and co-workers, has made a significant impact on our understanding of protein structure and conformation (Ramachandran et al., 1963; Ramakrishnan & Ramachandran, 1965; Ramachandran & Sasisekharan, 1968). The 2D plot of main chain torsion angles, with  $\varphi$  on the x axis and  $\psi$  on the y axis, describes the available conformational space for proteins in general and residues in particular. Initially using the van der Waals steric criteria, it was proposed that there were two distinct types of map, Gly (achiral residue) and general (representing the remaining chiral residues). Subsequently examining the residue-wise population statistics in protein structures led to the introduction of multiple types of Ramachandran maps corresponding to the different steric environments of residues Gly, Val/Ile (aliphatic  $C^{\beta}$  branched), pre-Pro (X-Pro, i.e. residue preceding Pro), trans-Pro, cis-Pro and general (representing the remaining 16 amino acids) (Chen et al., 2010; Williams et al., 2018).

As the distribution of torsion angles among proteins is not uniform, Karplus and co-workers proposed yet another type of 3D map with the z axis representing the frequency of each  $(\varphi, \psi)$  bin in the 2D map (Hollingsworth & Karplus, 2010). The four regions (favoured or core/allowed/generously allowed/disallowed) or three regions (favoured/allowed/disallowed or fully allowed/partially allowed/disallowed) are widely acknowledged in the literature (Ramachandran & Sasisekharan, 1968; Morris  $et\ al.$ , 1992; Chen  $et\ al.$ , 2010). Even two regions, core and non-core, have also been proposed (Kleywegt & Jones, 1996). The corresponding boundaries of



these regions in the map were proposed, and two types of boundary are prevalent: (i) steric criterion or energy-based (Ramachandran *et al.*, 1963; Ramakrishnan & Ramachandran, 1965; Ramachandran & Sasisekharan, 1968; Carrascoza *et al.*, 2014) and (ii) statistical probability-based using high-resolution structures available in the Protein Data Bank (PDB; Berman *et al.*, 2000) (Morris *et al.*, 1992; Laskowski *et al.*, 1993; Kleywegt & Jones, 1996; Anderson *et al.*, 2005; Park *et al.*, 2023; Chen *et al.*, 2010; Lovell *et al.*, 2003).

The first attempt to display steric plots using a computer program was made by Ramakrishnan and co-workers, who developed many in-house Fortran programs for this purpose (Srinivasan, 2019). Subsequently, several tools and web servers were developed such as *PROCHECK* (Laskowski *et al.*, 1993), *WHATIF* (Vriend, 1990), *PDBsum* (Laskowski *et al.*, 1997), *STING* (Neshich *et al.*, 2003), *RP on web* (Sheik *et al.*, 2002) and *MolProbity* (Chen *et al.*, 2010; Williams *et al.*, 2018). Additionally, commercial and open access molecular modelling and crystallographic refinement programs such as *DeepView*, *Rasmol*, *Pymol* (*Dynoplot*), *VMD*, *COOT*, *CCP4* (*Rampage*), Schrödinger *Maestro* and *BIOVIA Discovery Studio* also provide add-on utilities to draw maps (Sayle & Milner-White, 1995; Guex & Peitsch, 1997; Emsley & Cowtan, 2004; Schrödinger, 2023).

To the best of our knowledge, existing online or in-built software utilities are not flexible enough to draw many different types of 2D or 3D Ramachandran maps to display conformational excursions and transitions obtained in simulation and NMR structures, or for designed peptides containing non-standard residues. To address these issues, we have developed a utility, *RamPlot*, to draw assorted types of Ramachandran maps via either online or offline use. This utility is flexible and accepts many different input formats including flat files of torsion angles, and it generates a variety of maps and calculations.

#### 2. Method

The map can be drawn using various types of input:

- (i) As PDB code. To access all experimental structures, the web server is interfaced with the PDB archive.
- (ii) By uploading a PDB file or .mmcif file from a local computer. Users having other structural formats such as Mol2 or SDF may use the *OpenBabel* API link (https://openbabel.org/) to convert into PDB format.
- (iii) Using main chain and side chain torsion angle flat file format for peptides  $(\varphi, \psi / \varphi, \psi, \chi)$  containing standard or non-standard residues.
- (iv) Using *GROMACS* (Abraham *et al.*, 2015) simulation trajectory files (.tpr and .xtc).

The front end of the web server was developed using HTML, CSS, Bootstrap and JavaScript to display the Ramachandran plot, and the back end was developed using PHP and Python. *Biopython* (Cock *et al.*, 2009), *NumPy* (Harris *et al.*, 2020), *pandas* (https://pandas.pydata.org/) and *Matplotlib* (Hunter, 2007) packages were used to calculate and plot

torsion angles. The web server has been tested on all major browsers like Google *Chrome*, Microsoft *Edge*, Apple *Safari* and Mozilla *Firefox*. *RamPlot* runs on a dedicated server in the cloud.

The regional boundaries for six different categories of 2D Ramachandran maps were statistically estimated in MolProbity using the Top8000 reference database containing 7957 protein chains at 70% identity level: 98% in favoured, 1.8% in allowed and 0.2% in disallowed regions (Lovell et al., 2003; Williams et al., 2018). This remains more or less the same with the latest release of the Top2018 data set (8307 chains at 30% identity level; Williams et al., 2022). For Asx maps (see below), the kernel density estimation (kde) Python library was used with periodic boundary conditions imposed to estimate the probability density function (PDF) and generate smooth contours (Scott, 1992). The present server uses the same boundaries as obtained in *MolProbity* using the Top8000 reference data set. To validate these regional boundaries in the Ramachandran statistical map, we took a noise-free highfidelity data set (Set-1; resolution  $\leq 2 \text{ Å}$  and  $R_{\text{free}} \leq 0.25$ ) containing 72715 entries having 85309 chains. To obtain a non-redundant (non-homologous) data set, we clustered 85309 chain sequences taking a similarity threshold of 30% or more using MMseqs2 (Mirdita et al., 2019) and obtained 39295 representative chains (47.06%) constituting a non-redundant data set. In validation Set-1, even at its most stringent level (30% sequence identity), there were about five times as many chains as in Top8000, and hence we proceeded with the 30% sequence identity. RSRZ (real-space R value Z score) outlier residues having RSRZ > 2 were identified from wwPDB reports and a filtered Set-1 was also created (Jones et al., 1991; Kleywegt et al., 2004).

To calculate the main chain torsion angles of non-standard residues available in the PDB, an in-house Python script was written. To plot a map for a non-standard residue such as Aib, 61 crystal structures (89 peptide chains) containing Aib in the PDB were downloaded [Fig. S4(c) in the supporting information]. For other non-standard residues such as those deposited in the Cambridge Structural Database (CSD; Groom et al., 2016), a separate torsion angle file in the prescribed format should be provided. To analyse the ensemble of conformations obtained in the molecular dynamics (MD) simulation, particularly the conformational excursions and transitions of a specific residue, we use the GROMACS trajectory (.xtc) and topology (.tpr) files as input. Trajectory files obtained from other open source and commercial simulation programs can also be used, provided they are converted into GROMACS format using VMD or other similar software. These files are parsed using the MDAnalysis Python package (Michaud-Agrawal et al., 2011) to extract the structures from the trajectory. We then calculate the torsion angles of the residues and plot them using Biopython and Matplotlib. This allows us to visualize the flexibility and conformational changes of a residue over time, providing insights about its role in the overall protein dynamics. Additionally, one can draw a conformational energy contour map (utility provided on a separate page entitled

**Table 1**Torsion angle statistics in favoured, allowed and disallowed regions for each residue for validation Set-1.

The values indicate the occurrence of a particular residue in each of the regions. The percentage of the data is shown in brackets.

Serial No.	Residue	No. in favoured region (%)	No. in allowed region (%)	No. in disallowed region (%)	Total
1	Alanine	695937 (98.35)	10840 (1.53)	812 (0.11)	707589
2	Arginine	415119 (98.24)	6952 (1.65)	476 (0.11)	422547
3	Asparagine	337662 (95.34)	15828 (4.47)	690 (0.19)	354180
4	Aspartic acid	477757 (95.92)	19280 (3.87)	1064 (0.21)	498101
5	cis-Proline	22327 (97.82)	420 (1.84)	77 (0.34)	22824
6	Cysteine	110851 (97.37)	2891 (2.54)	99 (0.09)	113841
7	Glutamic acid	538852 (98.61)	6910 (1.26)	712 (0.13)	546474
8	Glutamine	311802 (98.48)	4426 (1.40)	385 (0.12)	316613
9	Glycine	659489 (97.69)	14399 (2.13)	1172 (0.17)	675060
10	Histidine	194777 (97.01)	5671 (2.82)	326 (0.16)	200774
11	Isoleucine	459979 (98.29)	7519 (1.61)	499 (0.11)	467997
12	Leucine	761415 (99.04)	7039 (0.92)	375 (0.05)	768829
13	Lysine	466297 (98.26)	7565 (1.59)	685 (0.14)	474547
14	Methionine	161126 (98.63)	2127 (1.30)	119 (0.07)	163372
15	Phenylalanine	336957 (98.30)	5608 (1.64)	206 (0.06)	342771
16	pre-Proline	367372 (98.09)	6413 (1.71)	730 (0.19)	374515
17	Serine	508686 (97.22)	13456 (2.57)	1085 (0.21)	523227
18	Threonine	470186 (98.23)	8075 (1.69)	377 (0.08)	478638
19	trans-Proline	388040 (97.88)	7568 (1.91)	849 (0.21)	396457
20	Tryptophan	126689 (98.25)	2182 (1.69)	79 (0.06)	128950
21	Tyrosine	302591 (98.12)	5600 (1.82)	191 (0.06)	308382
22	Valine	597078 (98.02)	11136 (1.83)	906 (0.15)	609120
	Total	8710989 (97.93)	171905 (1.93)	11914 (0.13)	8894808

'Energy Plots'), if molecular or quantum mechanics based coordinate scan data (*i.e.*  $\varphi$ ,  $\psi$  and energy) are supplied.

A sample of all the torsion angle file formats is available on the submission page. Scripts are available on GitHub (https://github.com/mayank2801/ramplot). The program is also available at the PyPI repository (https://pypi.org/project/ramplot/), from where it can be downloaded and installed with the command 'pip install ramplot'. A manual page explaining the required inputs and outputs is also provided.

#### 3. Results and discussion

To display various types of allowed/disallowed regions in a Ramachandran map, two distinct types of boundaries are prevalent. One is obtained using van der Waals radii and steric criteria (*i.e.* hard-sphere approximation-based) to determine fully allowed/partially allowed/disallowed regions as originally proposed (Ramachandran *et al.*, 1963; Ramachandran & Sasisekharan, 1968; Ramakrishnan & Ramachandran, 1965).

Along the same lines, such boundaries can also be obtained using coordinate (torsion angle) scans with regional contours based on molecular mechanics or quantum mechanics energy calculations (Ramachandran & Sasisekharan, 1968; Carrascoza et al., 2014). The second type is based on statistical approaches, where a  $360^{\circ} \times 360^{\circ}$  2D map is divided into about  $10^{\circ} \times 10^{\circ}$  or even finer bins. The probability of occurrence in each bin is decided and then smooth contours are drawn using a density-dependent smoothing function with a periodic boundary condition to generate favoured, allowed or disallowed boundaries as displayed in PROCHECK, MolProbity and other programs (Morris et al., 1992; Laskowski et al., 1993; Kleywegt & Jones, 1996; Lovell et al., 2003; Anderson et al., 2005; Chen et al., 2010). In MolProbity, which is based on the Top8000 reference database of protein structures containing 7957 chains, the residues were grouped into six different categories, (i) Gly (achiral), (ii) Val/Ile (aliphatic  $C^{\beta}$  branched), (iii) pre-Pro (X-Pro, i.e. residue preceding Pro), (iv) trans-Pro, (v) cis-Pro and (vi) general (representing the remaining 16

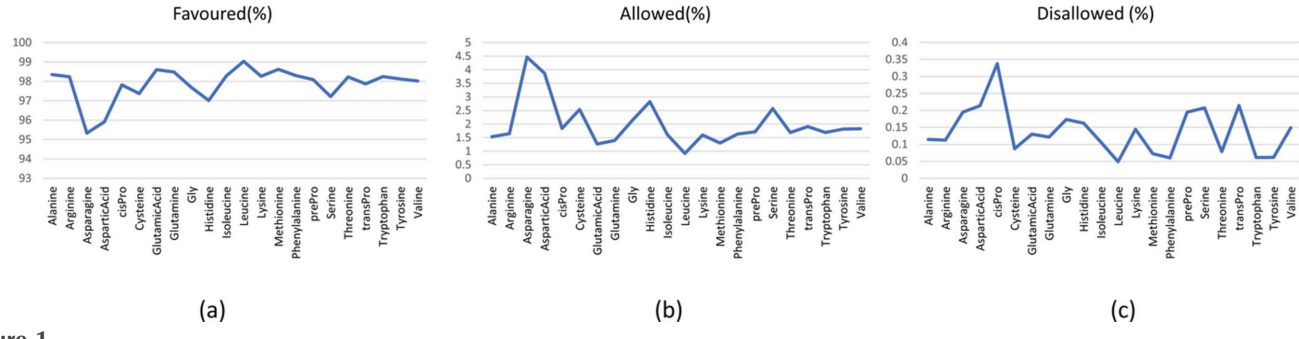


Figure 1
Percentage occurrence of torsion angles in (a) favoured, (b) allowed and (c) disallowed regions for all residues. The significant deviation for Asx (Asn/Asp) is evident in the curves.

residues) (Williams et al., 2018). As mentioned above, about 98% torsion angles were considered in the favoured region. 1.8% in the allowed region (amounting to a total of 99.8% in allowed categories), and 0.2% in the outlier or disallowed region. Using the large non-redundant validation Set-1 of 39295 chains, we plotted maps for all six of these categories, and found similar statistics for the residues in the favoured, allowed and disallowed regions (Table 1 and Fig. S1). Specifically, the present analysis reveals 97.93% of residues in the favoured region, 1.93% in the allowed region and 0.13% in the disallowed region, in conformity with what was reported earlier (Williams et al., 2018). For further validation Set-1 was filtered with RSRZ outliers, i.e. residues with RSRZ > 2 were removed from Set-1 (Kleywegt et al., 2004; Jones et al., 1991). In the filtered data set, 98.10% of the residues were found in the favoured region, 1.81% in the allowed region and only 0.09% in the disallowed region, suggesting that the removal of these outlier residues did not lead to any significant changes. Residue-wise statistics for RSRZ-filtered Set-1 are provided in Table S1.

The percentage occurrence of torsion angles in the favoured, allowed and disallowed regions is shown in Fig. 1. In these graphs, residues Asn and Asp turn out to be outliers. Examining the frequency distribution, we noticed significant

differences in the torsion angle distributions of Asp and Asn (Table 1 and Fig. 1). These amino acids have 2-3% less occurrence in the favoured region [Fig. 1(a)] and 2–3% more in the allowed region [Fig. 1(b)] compared with the distributions of other residues [Fig. 1(c)]. This distinct observation for Asx (Asn/Asp) stems from multiple factors (Kumar & Rathore, 2023). Residues Asn, Asp, Gln and Glu (and also Ser and Thr) possess side chains similar to the main chain, enabling them to participate in hydrogen bonding with the main chain through side chain carbonyl oxygen atoms and/or amides, as either donor or acceptor, and to stabilize various kinds of  $\alpha$ -,  $\beta$ - and  $\gamma$ -turn mimics. Several examples of Asx-(Asp/Asn) and ST-turns, stabilized by (side chain)-(main chain) interactions, have been reported and characterized (Kumar & Rathore, 2023; Duddy et al., 2004; Kalmankar et al., 2014). The (side chain)–(main chain) interactions to stabilize turn mimics offer energetic compensation for such residues to be in the disallowed conformation. Among such residues, Asn/ Asp have demonstrated the highest propensity to form hydrogen-bonded turn mimics, followed by Ser/Thr residues. The side chains of Gln and Glu have polar atoms at the remotely located  $\varepsilon$ -position (compared with Asp/Asn) and therefore do not show a significant preference to form such hydrogen-bonded turns. Similarly, the polar atoms of the Arg

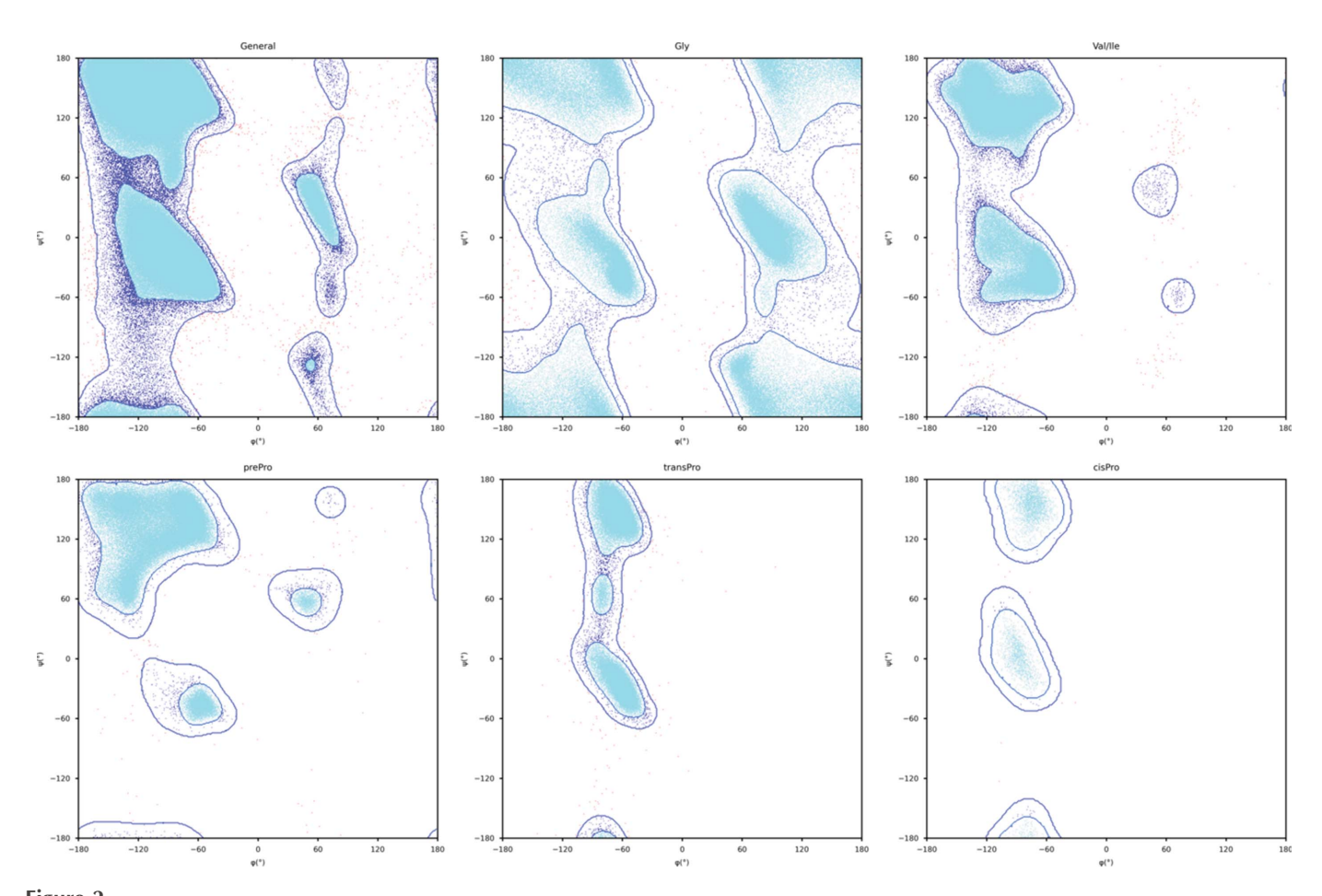


Figure 2
Two-dimensional Ramachandran plot of the Top8000 data set in six distinct categories: general case (Ala representing the remaining 16 amino acids), Gly, Val/Ile, pre-Pro, trans-Pro and cis-Pro. Cyan, blue and red dots represent torsion angles of favoured, allowed and disallowed regions, respectively.

and Lys side chains cannot participate in such hydrogen bonding because their donor atoms have a greater separation from the main chain. This analysis suggests that an additional seventh distinct category of the 2D/3D Ramachandran map, namely Asx (Asn/Asp), needs to be defined. The map for Asx using the Top8000 data set is shown in Fig. S2 (Williams et al., 2022). Smooth contour criteria were applied to ensure that 98% of residues were enclosed within the favoured region and a total of 99.8% within the allowed category, as done earlier (Chen et al., 2010; Lovell et al., 2003; Williams et al., 2022). After validation with Set-1 for Asn, 97.78% of residues were in the favoured region, 2.03% in the allowed region and 0.19% in the disallowed region. Similarly for Asp, 98.03% of residues were in the favoured region, 1.74% in the allowed region and 0.21% in the disallowed region (Fig. S2). These distributions are consistent with the preferences observed for other residues in these regions.

We now list the functionalities that have been included in the *RamPlot* server.

#### 3.1. Two- and three-dimensional maps of various categories

The program generates conventional 2D and 3D maps (Ala and Gly) as well as all six categories of Ramachandran maps – Gly, Val/Ile, pre-Pro, *trans*-Pro, *cis*-Pro and general (representing the remaining 16 amino acids). Asx and other types of maps such as heat maps can also be plotted from the 'More Plots' option. One of the important features is to display 3D maps (frequency along the third *z* axis or even as heat maps) in different steric environments. Two- and three-dimensional Ramachandran plots in six distinct categories for the Top8000

data set are shown in Figs. 2 and 3, respectively. Ramachandran maps for the seventh category, ASX (Asn/Asp), are displayed in Fig. S2. Three-dimensional maps provide complimentary knowledge regarding conformational trends. The difference in conformational preferences in different steric environments such as between Ala (all 16 residues except Gly/Val/Ile/Pro), C<sup>β</sup>-branched aliphatic residues, Val/ Ile and pre-Pro is obvious in the 3D maps. In Val/Ile the  $\beta$ -region has proportionately more population and a near absence of the left-handed helical region in contrast to Ala. Similarly, pre-Pro has an almost equal ratio of population in the helical and sheet regions. The asymmetric distribution of glycine is evident in the 3D map. One may also draw the textbook versions of the conventional Ramachandran plot (Ala and Gly instead of the six different categories of maps) as shown in Figs. S3(a) and S3(b) for 2D and 3D maps, respectively.

#### 3.2. Ramachandran map for non-standard residues

One of the novel options available in *RamPlot* is to plot a Ramachandran map of non-standard residues using a prescribed flat file input format, as existing *Biopython* scripts are not able to deal with non-standard residues. Two- and three-dimensional Ramachandran plots of a representative non-standard amino acid, aminoisobutyric acid (Aib), observed in peptides are shown in Figs. S4(a) and S4(b), respectively. Aib has been extensively studied as a prototypical example to investigate the effect of introducing steric constraints (such as  $C^{\alpha,\alpha}$  dialkylated glycines) in the peptide backbone. This could prove to be a viable strategy to narrow

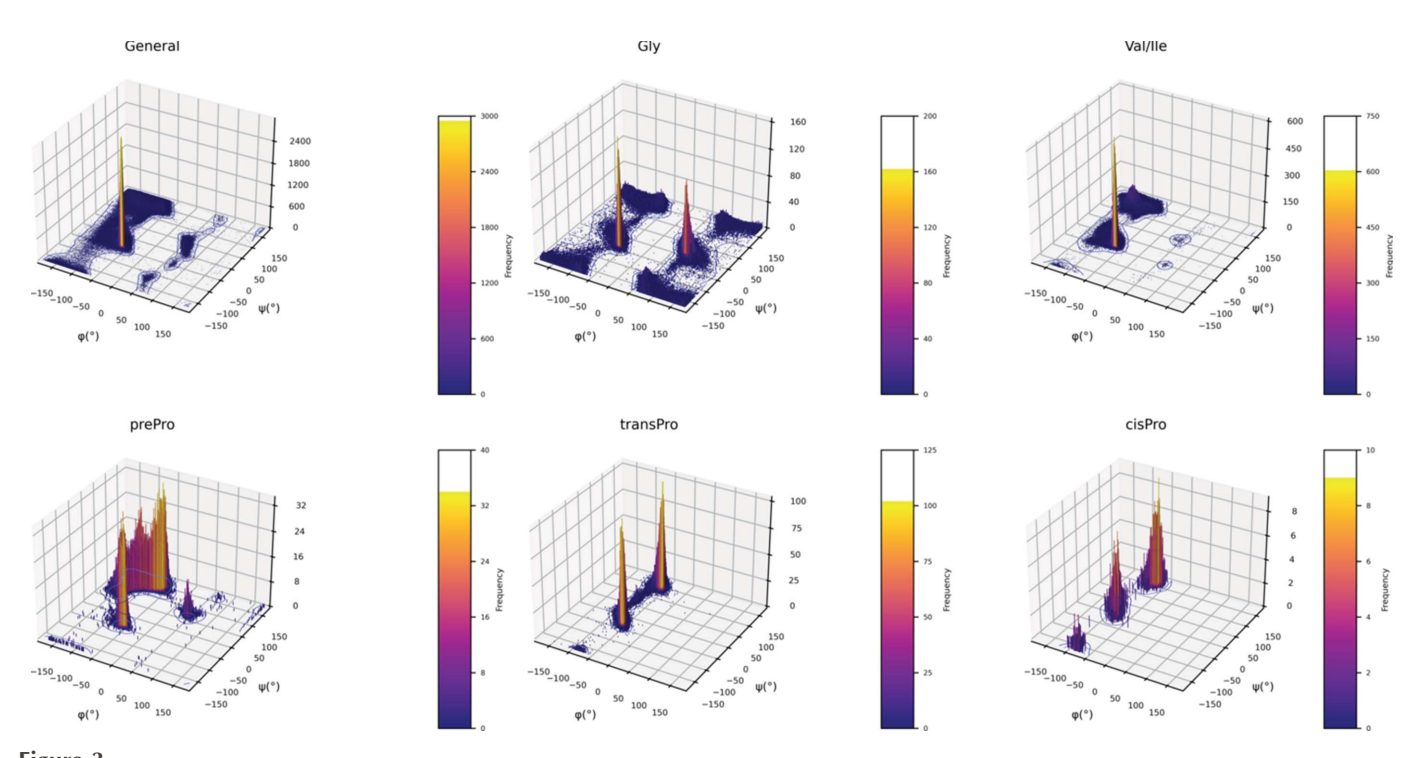


**Figure 3**Three-dimensional Ramachandran plots of the Top8000 data set in six distinct categories: general case (Ala representing the remaining 16 amino acids), Gly, Val/Ile, pre-Pro, *trans*-Pro and *cis*-Pro. Vertical bars on the *z* axis represent the frequency of occurrence of torsion angles.

634 Kumar and Rathore • RamPlot J. Appl. Cryst. (2025). 58, 630–636

down the available conformational space into useful helical and sheet regions. The map for non-coded amino acids serves as a very useful visual add on for a quick analysis of the conformational tendency of such residues. In Fig. S4, the population is predominantly concentrated in right-hand  $3_{10}$  or  $\alpha$ -helical regions ( $\varphi=-66.8$  to  $-38.8^{\circ}$ ,  $\psi=-61.6$  to  $-10.0^{\circ}$ ), and to a lesser extent in the left-hand region ( $\varphi=46.9$  to  $63.4^{\circ}$ ,  $\psi=23.3$  to  $56.4^{\circ}$ ). This makes it strongly helicogenic to nucleate or stabilize secondary structures such as turns and helices in peptide *de novo* design strategies (Karle, 2002; Castro *et al.*, 2023).

#### 3.3. Conformational excursion

The visualization of sampled conformations and transitions observed during MD simulations, and in experimentally observed NMR structures, helps in gaining mechanistic insight into the molecular processes. An option has been provided in RamPlot to draw residue-specific conformation excursions extracted from simulation trajectories. Fig. S5 shows an example output using a conformational trajectory for residue Met (residue number 793) in chain A of the EGFR kinase domain (PDB entry 5ug9; Planke  $et\ al.$ , 2017) during a 200 ns simulation run. The map highlights the large conformational fluctuation of the residue occurring in the helical region with a transition into the  $\beta$ -sheet region of a significant duration observed.

### 3.4. Analysis of preferred backbone-dependent rotamers and $\omega$ -amino acids

The z axis of a 3D map apart from a frequency plot can also be utilized to plot and examine the variation in the third torsion angles such as side-chain torsion angles ( $\chi^1$ ,  $\chi^2$  etc.) or any property varying with backbone torsion angles. A representative plot [Fig. S6(b)] shown for Ser indicates that g+ followed by g— are the most preferred rotamers for helical and extended conformations. Such plots help in gaining insights on preferred rotamers for particular backbone conformations (Chakrabarti & Pal, 2001).

RamPlot can also be used to find the preferred conformation of non-standard residues having extended backbones such as  $\omega$ -amino acids. They occur in nature as metabolically derived products and, due to the extended flexibility of their backbone, they have been explored in the design of novel secondary and super-secondary structure folds (Kishore, 2004). As an example, the conformational preference of ( $\varphi$ ,  $\theta$  and  $\psi$ ) of one of the  $\omega$ -amino acids,  $\beta$ -alanine (-N-CB-CA-CO-), is shown in Fig. S6( $\alpha$ ). The conformational tendency of  $\beta$ -Ala in this 3D plot, where the population is concentrated around an extended region of ( $\varphi$  and  $\psi$ ) and  $\theta$  (torsion angle about CB-CA) surrounding (g+ or g-), is clearly manifested.

The present online utility accepts many types of input file formats (.pdb, .mmcif, .csv and flat file), displays graphs in various output formats (.png, .svg and .jpg) and provides the results of calculations for analysis. A detailed description of torsion angle calculations is provided in a downloadable text file, which helps the user examine residue

occurrence in various regions of the Ramachandran map. A list of main chain and side chain torsion angles is also saved in a .csv file. The results of the output file are self-explanatory and a manual is also provided. The statistics in various allowed and disallowed regions are of immense help for model building, structure validation, peptide design and various modelling tasks.

#### 4. Conclusion

RamPlot is a useful tool to display various categories of  $(\varphi, \psi)$  plots and to study the conformations of proteins and peptides in local regions. The utility, available to operate either online or offline, is a collection of many small applications to plot a variety of Ramachandran maps: 2D and 3D plots of standard maps as well as several distinct categories of maps, namely Gly, Val/Ile, pre-Pro, *trans*-Pro, *cis*-Pro and general. In this work, we have also highlighted another distinct category of  $(\varphi, \psi)$  map, Asx (Asn/Asp).

RamPlot may be used to plot Ramachandran maps for non-standard residues to examine their conformational preferences. Such knowledge is useful in the *de novo* design of peptides and proteins. Another application is to examine backbone-dependent rotamer preferences for standard and non-standard residues.

Conformational excursions and transitions are deciphered using molecular dynamics and NMR techniques. Using the molecular dynamics trajectory, *RamPlot* can draw a map displaying the conformational landscape of specified residues.

The *RamPlot* utility, which is able to produce a variety of plots using multiple types of input formats from various sources, could also be flexible for the user to draw, interpret and analyse conformation maps in miscellaneous situations.

The package is available at https://www.ramplot.in/. Scripts are also available for offline use from the PyPI repository and GitHub (https://github.com/mayank2801/ramplot). It can be installed on a local computer using 'pip install ramplot'. Further installation and execution instructions are described in the README file.

#### **Acknowledgements**

Infrastructure support to the department by DST-FIST SR/FST/LS-1/2023/1176 is gratefully acknowledged. MK thanks the UGC for a Non-NET PhD Fellowship.

#### Conflict of interest

The authors declare no conflicts of interest.

#### References

Abraham, M. J., Murtola, T., Schulz, R., Páll, S., Smith, J. C., Hess, B. & Lindahl, E. (2015). *SoftwareX*, **1–2**, 19–25.

Anderson, R. J., Weng, Z., Campbell, R. K. & Jiang, X. (2005).
Proteins, 60, 679–689.

- Berman, H. M., Westbrook, J., Feng, Z., Gilliland, G., Bhat, T. N., Weissig, H., Shindyalov, I. N. & Bourne, P. E. (2000). *Nucleic Acids Res.* **28**, 235–242.
- Carrascoza, F., Zaric, S. & Silaghi-Dumitrescu, R. (2014). *J. Mol. Graphics Modell.* **50**, 125–133.
- Castro, T. G., Melle-Franco, M., Sousa, C. E. A., Cavaco-Paulo, A. & Marcos, J. C. (2023). *Biomolecules*, 13, 981.
- Chakrabarti, P. & Pal, D. (2001). Prog. Biophys. Mol. Biol. 76, 1–102.
  Chen, V. B., Arendall, W. B., Headd, J. J., Keedy, D. A., Immormino, R. M., Kapral, G. J., Murray, L. W., Richardson, J. S. & Richardson, D. C. (2010). Acta Cryst. D66, 12–21.
- Cock, P. J. A., Antao, T., Chang, J. T., Chapman, B. A., Cox, C. J., Dalke, A., Friedberg, I., Hamelryck, T., Kauff, F., Wilczynski, B. & de Hoon, M. J. L. (2009). *Bioinformatics*, 25, 1422–1423.
- Duddy, W. J., Nissink, J. W. M., Allen, F. H. & Milner-White, E. J. (2004). *Protein Sci.* 13, 3051–3055.
- Emsley, P. & Cowtan, K. (2004). Acta Cryst. D60, 2126-2132.
- Groom, C. R., Bruno, I. J., Lightfoot, M. P. & Ward, S. C. (2016). Acta Cryst. B72, 171–179.
- Guex, N. & Peitsch, M. C. (1997). Electrophoresis, 18, 2714-2723.
- Harris, C. R., Millman, K. J., van der Walt, S. J., Gommers, R., Virtanen, P., Cournapeau, D., Wieser, E., Taylor, J., Berg, S., Smith, N. J., Kern, R., Picus, M., Hoyer, S., van Kerkwijk, M. H., Brett, M., Haldane, A., del Río, J. F., Wiebe, M., Peterson, P., Gérard-Marchant, P., Sheppard, K., Reddy, T., Weckesser, W., Abbasi, H., Gohlke, C. & Oliphant, T. E. (2020). *Nature*, **585**, 357–362.
- Hollingsworth, S. A. & Karplus, P. A. (2010). *Biomol. Concepts*, 1, 271–283.
- Hunter, J. D. (2007). Comput. Sci. Eng. 9, 90-95.
- Jones, T. A., Zou, J.-Y., Cowan, S. W. & Kjeldgaard, M. (1991). Acta Cryst. A47, 110–119.
- Kalmankar, N. V., Ramakrishnan, C. & Balaram, P. (2014). *Proteins*, **82**, 1101–1112.
- Karle, I. L. (2001). Biopolymers, 60, 351-365.
- Kishore, R. (2004). Curr. Protein Pept. Sci, 5, 435-455.
- Kleywegt, G. J., Harris, M. R., Zou, J., Taylor, T. C., Wählby, A. & Jones, T. A. (2004). Acta Cryst. D60, 2240–2249.
- Kleywegt, G. J. & Jones, T. A. (1996). Structure, 4, 1395-1400.
- Kumar, M. & Rathore, R. S. (2023). Biochim. Biophys. Acta, 1867, 130493.
- Laskowski, R. A., Hutchinson, E. G., Michie, A. D., Wallace, A. C., Jones, M. L. & Thornton, J. M. (1997). Trends Biochem. Sci. 22, 488–490.
- Laskowski, R. A., MacArthur, M. W., Moss, D. S. & Thornton, J. M. (1993). J. Appl. Cryst. 26, 283–291.
- Lovell, S. C., Davis, I. W., Arendall, W. B., de Bakker, P. I. W., Word, J. M., Prisant, M. G., Richardson, J. S. & Richardson, D. C. (2003). Proteins, 50, 437–450.

- Michaud-Agrawal, N., Denning, E. J., Woolf, T. B. & Beckstein, O. (2011). *J. Comput. Chem.* **32**, 2319–2327.
- Mirdita, M., Steinegger, M. & Söding, J. (2019). *Bioinformatics*, 35, 2856–2858.
- Morris, A. L., MacArthur, M. W., Hutchinson, E. G. & Thornton, J. M. (1992). *Proteins*, **12**, 345–364.
- Neshich, G., Togawa, R. C., Mancini, A. L., Kuser, P. R., Yamagishi, M. E. B., Pappas, G., Torres, W. V., Fonseca e Campos, T., Ferreira, L. L., Luna, F. M., Oliveira, A. G., Miura, R. T., Inoue, M. K., Horita, L. G., de Souza, D. F., Dominiquini, F., Álvaro, A., Lima, C. S., Ogawa, F. O., Gomes, G. B., Palandrani, J. F., dos Santos, G. F., de Freitas, E. M., Mattiuz, A. R., Costa, I. C., de Almeida, C. L., Souza, S., Baudet, C. & Higa, R. H. (2003). *Nucleic Acids Res.* 31, 3386–3392.
- Park, S. W., Lee, B. H., Song, S. H. & Kim, M. K. (2023). J. Struct. Biol. 215, 107939.
- Planken, S., Behenna, D. C., Nair, S. K., Johnson, T. O., Nagata, A., Almaden, C., Bailey, S., Ballard, T. E., Bernier, L., Cheng, H., Cho-Schultz, S., Dalvie, D., Deal, J. G., Dinh, D. M., Edwards, M. P., Ferre, R. A., Gajiwala, K. S., Hemkens, M., Kania, R. S., Kath, J. C., Matthews, J., Murray, B. W., Niessen, S., Orr, S. T., Pairish, M., Sach, N. W., Shen, H., Shi, M., Solowiej, J., Tran, K., Tseng, E., Vicini, P., Wang, Y., Weinrich, S. L., Zhou, R., Zientek, M., Liu, L., Luo, Y., Xin, S., Zhang, C. & Lafontaine, J. (2017). *J. Med. Chem.* **60**, 3002–3019.
- Ramachandran, G. N., Ramakrishnan, C. & Sasisekharan, V. (1963). J. Mol. Biol. 7, 95–99.
- Ramachandran, G. N. & Sasisekharan, V. (1968). *Adv. Protein Chem.* **23**, 283–437.
- Ramakrishnan, C. & Ramachandran, G. N. (1965). *Biophys. J.* **5**, 909–933.
- Sayle, R. A. & Milner-White, E. J. (1995). *Trends Biochem. Sci.* **20**, 374–376.
- Schrödinger (2023). Maestro. Schrödinger LLC, New York, USA.
- Scott, D. W. (1992). Multivariate density estimation: theory, practice, and visualization. New York: John Wiley & Sons.
- Sheik, S. S., Sundararajan, P., Hussain, A. S. Z. & Sekar, K. (2002). *Bioinformatics*, **18**, 1548–1549.
- Srinivasan, N. (2019). Protein Sci. 28, 1920-1922.
- Vriend, G. (1990). J. Mol. Graph. 8, 52-56.
- Williams, C. J., Headd, J. J., Moriarty, N. W., Prisant, M. G., Videau, L. L., Deis, L. N., Verma, V., Keedy, D. A., Hintze, B. J., Chen, V. B., Jain, S., Lewis, S. M., Arendall, W. B., Snoeyink, J., Adams, P. D., Lovell, S. C., Richardson, J. S. & Richardson, D. C. (2018). *Protein Sci.* 27, 293–315.
- Williams, C. J., Richardson, D. C. & Richardson, J. S. (2022). Protein Sci. 31, 290–300.